Structure and electrical properties of $Co_n(CoO)_{100-n}$ thin-film composites

© *A.V. Sitnikov, V.A. Makagonov, Y.E. Kalinin, S.B. Kushchev, V.A. Foshin*

Voronezh State Technical University,
394026 Voronezh, Russia
e-mail: vlad_makagonov@mail.ru

The electrical properties of $Co_n(CoO)_{100-n}$ composite thin films obtained by ion-beam sputtering of a composite target in an argon atmosphere and a mixed atmosphere of argon and oxygen $(98\%\,Ar + 2\%\,O_2)$ have been studied. It has been established that if oxygen is introduced into the deposition chamber, the position of the percolation threshold shifts towards lower concentrations of the metal phase. It is associated with the special morphology of the films, when small metal Co nanoparticles are located along the boundaries of larger CoO particles, as well as a decrease in the size of inclusions of the metal phase. Studies of the temperature dependences of the electrical resistivity of synthesized $Co_n(CoO)_{100-n}$ films have shown that when the metal phase content is up to the percolation threshold the dominant mechanism of charge transfer in the temperature range of $80-140\,K$ is the variable range hopping mechanism of conduction through localized states near the Fermi level, replaced by the nearest neighbors conductivity in the temperature range of $140-300\,K$. For beyond the percolation threshold $Co_n(CoO)_{100-n}$ thin films, the conductivity is determined by a network of metal granules and is characterized by a positive temperature coefficient of electrical resistance.

Keywords: Electrical conductivity, nanocomposites, percolation threshold, hopping conductivity.

DOI: 10.61011/TP.2023.11.57507.137-23

Introduction

Granulated nanocomposites consisting of metallic nanoparticles embedded in dielectric (SiO_2, Al_2O_3, MgO, ZrO_2) or semiconductor (In_2O_3, TiO_2, C, ZnO, $LiNbO_3$, SnO_2) matrices are still of interest of researchers both from the fundamental point of view and in terms of practical applications [1–3]. Cobalt composites in a dielectric matrix are of particular interest [4,5]. In particular, nanogranular Co-ZrO_2 films due to their soft magnetic properties are reported to be promising for practical applications such as dielectric layer to reduce eddy currents in high frequency converters designed for high currents and low voltages [6]. Most physical and chemical properties of these nanocomposites are strongly dependent on the production method, particle size and concentration, and chemical bond between atoms at the interface between Co nanoparticles and CoO matrix [7]. For synthesis of granulated nanomaterials, chemical methods — sol-gel method, electrochemical deposition, microemulsion method [8,9], as well as physical methods: magnetron sputtering, pulsed laser deposition, ion implantation, etc. are used [5,10,11]. However, the search for new methods for production of hybrid thin-film nanocomposites with pre-defined properties is still an essential task.

Despite the complex structure of nanogranular composites, production process by composite target sputtering and vapor-phase deposition methods is sufficiently simple and thoroughly studied. Such media are obtained using self-organization of two phases provided that they are mutually insoluble, contain no chemicals and have different surface energies [12]. While production of heterogenous structure in Co-CoO system from a composite target is not apparent. Usually, for production of nanocomposites by metal-dielectric self-organization methods, materials that do not interact chemically with each other, have limited solubility in each other or insoluble are used for the matrix and granules. In the discussed system, none of the criteria describe above is met.

This study is devoted to the synthesis and identification of behavior patterns of the electrical properties of nanogranular ferromagnetic cobalt composites in cobalt oxide matricproduced by the ion-beam composite target sputtering.

1. Samples and research procedures

The test samples were made by the ion-beam sputtering method using UVN-2M vacuum station, whose design is described in detail in [12]. Thin films with various cobalt content were produced using a composite water-cooled target made of cobalt and weighed quantities of CoO unevenly arranged on it, thus, samples with different ratio of Co and CoO were produced in a single process cycle. Synthesis of thin composite films was carried out both in argon atmosphere and in mixed argon-oxygen atmosphere $(98\%\,Ar + 2\%\,O_2)$. ST-50 ceramic polycrystalline glass, NaCl, plates were used as substrates. Thickness of the produced films was measured using MII-4 interferometer and was equal to $\sim 2\,\mu m$. Content of cobalt metal in
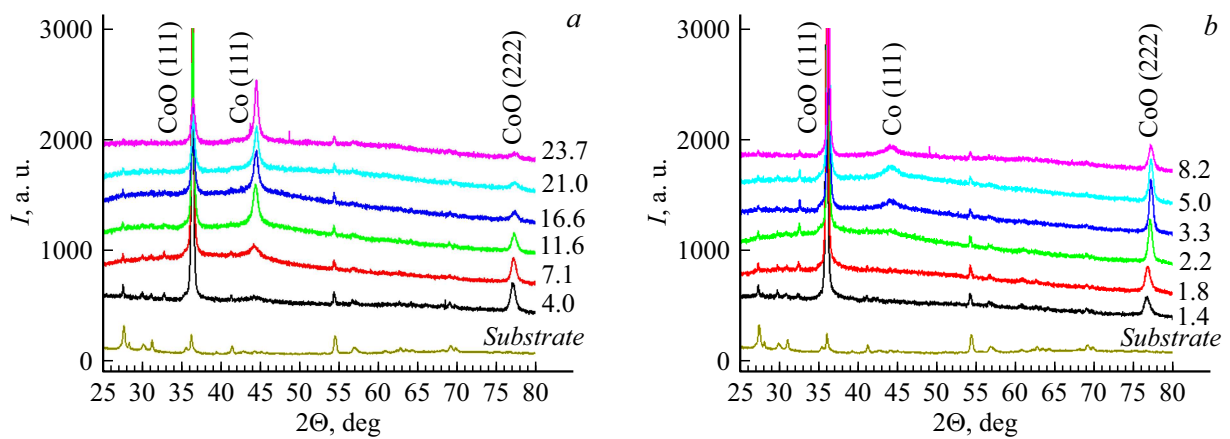
Figure 1. X-ray diffraction patterns of thin Co$_n$(CoO)$_{100-n}$ films produced by sputtering on ST-50 polycrystalline glass substrate in argon atmosphere (*a*) and mixed Ar + O$_2$ atmosphere (*b*). Numbers near the curves show the cobalt metal content in at.%.
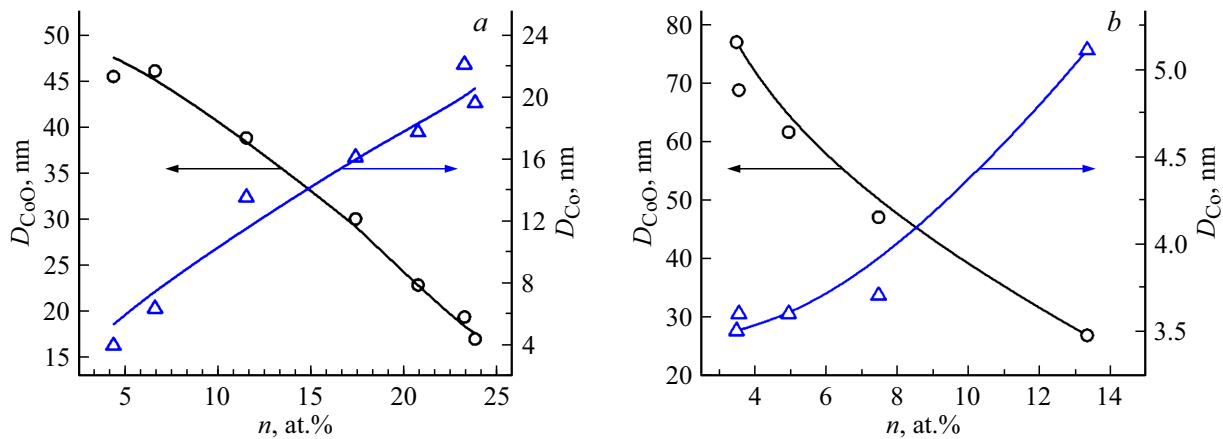

Figure 2. Average Co and CoO CSR for thin Co$_n$(CoO)$_{100-n}$ films produced by sputtering in argon atmosphere (*a*) and mixed Ar + O$_2$ atmosphere (*b*).

the samples measured by the X-ray phase analysis method varied from 2 to 24 at.%.

The structure of produced thin Co$_n$(CoO)$_{100-n}$ films, where *n* is the content of Co metal in at.%, was examined by the X-ray diffraction method using Bruker D2 Phaser ($\lambda_{CuK\alpha1} = 1.54$ Å) diffractometer and DIFFRAC.EVA 3.0 software with CDD PDF Release 2012 database and by transmission electron microscopy (TEM) method using Libra 120 and EMB-100BR electron microscopes. Thin films sputtered on a NaCl substrate were used in the composite structure examinations by the TEM method.

Concentration dependences of resistivity at room temperature and temperature dependences within 77−300 K were measured using a two-probe procedure.

2. Structure of thin Co$_n$(CoO)$_{100-n}$ films

Figure 1 shows X-ray diffraction patterns of thin Co$_n$(CoO)$_{100-n}$ films produced by sputtering in argon atmosphere (Figure 1, *a*) and mixed Ar + O$_2$ atmosphere ($P_{O_2} = 8 \cdot 10^{-6}$ Torr) (Figure 1, *b*). Target configuration

and power values on ion sources remained unchanged. The diffraction pattern analysis has shown that the produced films are two-phase and consist of textured cubic CoO (space group Fm-3m) and cobalt metal (space group Fm-3m) phases. Semiquantitative analysis of the cobalt metal phase was carried out using corundum numbers provided in ICDD PDF Release 2012 database cards (PDF 01-071-1178 for CoO and PDF 01-071-4651 for Co). For further analysis, the obtained estimated weight contents of Co metal were converted into atomic percentages and were from 2 to 24 at.% of Co metal. The presence of cubic modification of Co phase that is unstable at room temperature may be due to dimensional phase effect as well as to the impurity nature of the observed abnormal phase [13].

The average coherent scattering regions (CSR) estimated using the Scherer equation [14] and shown in Figure 2 suggest that the CoO grain size decreases and Co grain size increases with the growth of cobalt metal phase content. In this case, addition of oxygen during sputtering results in Co grain size decrease and CoO grain size increase.
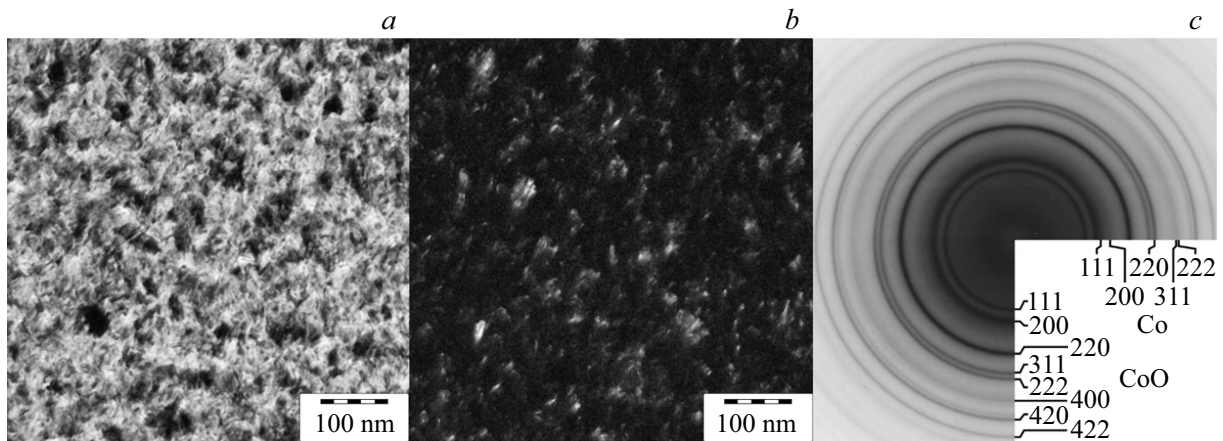
Figure 3. Bright field (*a*) and dark field in TEM image reflection 111 CoO (*b*) and a fragment of electron diffraction from thin $Co_{14}(CoO)_{86}$ film (*c*) condensed on the NaCl substrate in argon atmosphere.

The X-ray diffraction analysis has shown that average CoO CSR sizes for $Co_n(CoO)_{100-n}$ film change within a range from 15 to 80 nm, and for Co — are maximum 20 nm for samples sputtered in argon atmosphere and 5.5 nm for samples sputtered in .... atmosphere. $Ar + O_2$.

To study the structure by TEM methods, ~ 60 nm films were produced. Figure 3 shows the results of TEM examinations of thin $Co_{14}(CoO)_{86}$ film obtained by sputtering and deposition in argon atmosphere onto the NaCl substrate. TEM examinations have proved the conclusions that two phases are present (Co metal and CoO) (Figure 3).

Dark-field structure analysis in 111 CoO reflection (Figure 3, *b*) has shown that the matrix grain size in the film with such composition varies in a range from 3 to 15 nm. According to the electron diffraction pattern (Figure 3, *c*), a clearly pronounced texture$\langle 111 \rangle$ is observed for the CoO phase as evidenced by very intensive circular reflection 220. Reflections of the metallic phase are very weak and highly diffused suggesting a low number and size of these inclusions.

3. Electric properties of thin $Co_n(CoO)_{100-n}$ films

3.1. Dependence of resistivity and thermo-emf on the cobalt metal phase content

Figure 4 shows concentration dependences of resistivity of $Co_n(CoO)_{100-n}$ films measured at room temperature for the samples produced in inert atmosphere and with oxygen addition. For films produced in argon atmosphere, the resistivity decreases non-monotonically approximately by 7 orders of magnitude (curve *1* in Figure 4) with increasing metallic phase concentration.

The obtained dependence is typical for many heterogenous metal-dielectric systems [15], and considerable reduction of composite resistivity with increasing metallic phase

concentration is associated with transition from nonmetallic to metallic type of conductivity.

To determine the percolation threshold position, annealing of heterogenous $Co_n(CoO)_{100-n}$ systems were carried out at $T = 520$ K that did not resulted in significant change of morphology of these heterogenous systems. Figure 4 shows that annealing in low metallic phase concentration region results in increased resistivity of $Co_n(CoO)_{100-n}$ composites, and at high *n* values the resistivity decreases relative to the samples in initial state. Supposing that electrotransport of composites upstream of the percolation threshold is governed by the dielectric matrix, then it is apparent that decrease of defect concentration in CoO during heat treatment shall result in increasing resistivity of samples that is observed during the experiment. On the other hand, for samples downstream of the percolation threshold,
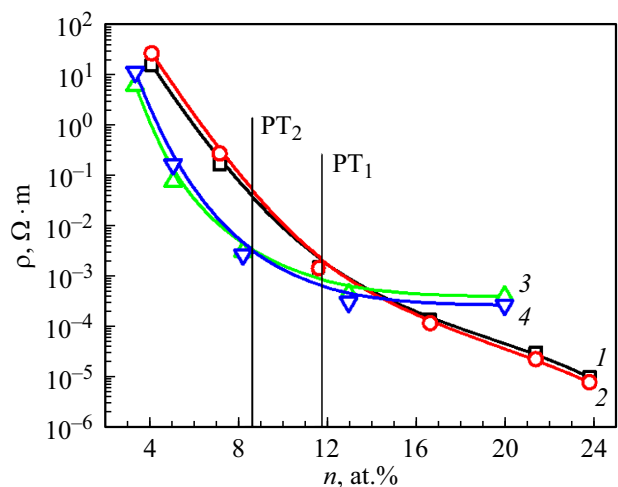

Figure 4. Dependences of resistivity on the cobalt metal content *n* measured for thin $Co_n(CoO)_{100-n}$ films produced by sputtering in argon atmosphere (*1, 2*) and mixed $Ar + O_2$ atmosphere (*3, 4*). *1, 3* — samples in initial state; *2, 4* — samples after heat treatment in vacuum $P_{res} = 2.5 \cdot 10^{-4}$ Torr at $T = 520$ K.

conductivity is provided over a grid of adjoining metallic granules. Then reduction of defects in the intercrystalline spaces between metallic nanoparticles during heat treatment shall result in decreasing resistance of the conducting metallic phase grid. In this case, the percolation threshold in Co$_n$(CoO)$_{100-n}$ composites may be estimated by the point of intersection of resistance-concentration dependences of the structures in initial and heat treated state. Estimates have shown that the percolation threshold accounts for 12.2 at.% of Co metal for the samples produced argon atmosphere (PT$_1$ in Figure 4) and for 8.3 at.% of Co metal for films produced with oxygen addition (PT$_2$ in Figure 4).

Analysis of the obtained dependences has identified several features that are not typical for nanocomposites. First, low concentration of the metallic phase (~ 12 at.%) corresponding to the percolation threshold compared with other metal-dielectric nanocomposites [16]. Second, oxygen addition results in percolation threshold displacement to the lower metallic phase concentration region and in reduction of the resistivity of Co$_n$(CoO)$_{100-n}$ composites for compounds upstream of the percolation threshold. At the same time, the resistivity in composites downstream of the percolation threshold produced in the mixed atmosphere is much higher than in the films synthesized in argon atmosphere.

To explain the identified resistivity behavior patterns, we shall return to the morphology of the synthesized composites. Wide variety of grain sizes in dielectric and metallic phases suggests uneven grain distribution in the composite. Thus, fine metallic Co granules shall be mainly concentrated at CoO grain boundaries. Such structure is schematically shown in Figure 5.
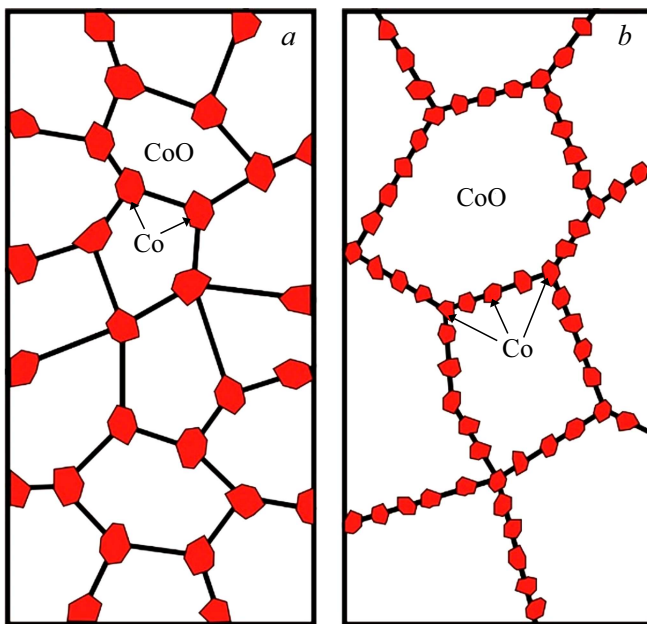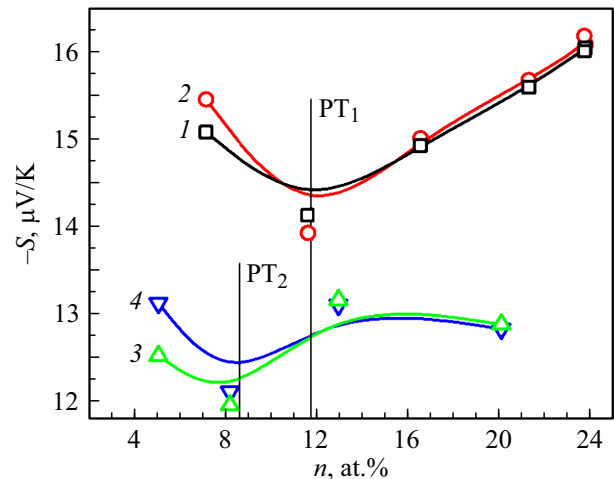
Figure 6. Dependences of thermo-emf on the cobalt metal content n measured for thin Co$_n$(CoO)$_{100-n}$ films produced by sputtering in argon atmosphere (*1, 2*) and mixed Ar + O$_2$ atmosphere (*3, 4*). *1, 3* — samples in initial state; *2, 4* — samples after heat treatment in vacuum $P_{res} = 2.5 \cdot 10^{-4}$ Torr at $T = 520$ K.

Oxygen addition into the synthesis of Co$_n$(CoO)$_{100-n}$ results in considerable reduction of Co grain sizes (Figure 2). It is apparent that the decrease in size of particles at the CoO grain interfaces results in decreasing average distance between metallic particles and, thus, increases the probability of tunnel current between them. In this case, it may be assumed that electrotransport of the produced composites is governed only by intergranular regions at the CoO interfaces, rather than by the whole volume of the heterogenous structure. Consequently, the conducting metallic grid is formed in a limited volume, for which very high metallic phase concentration compared with the whole sample volume is not required. This explains low metallic phase concentration ~ 12 at.% corresponding to the percolation threshold. As already mentioned, when oxygen in added, Co particle sizes decrease. Therefore, the number of particles increases at the same metallic phase concentration as for the samples produced in argon atmosphere resulting in more uniform particle distribution at the CoO grain boundaries and reduction of tunnel gaps between them. As a result, lower amount of the metallic phase is required to form a solid conducting metallic grid, i.e. with decreasing particle sizes the percolation threshold will shift towards the lower metallic phase concentration n in Co$_n$(CoO)$_{100-n}$. When the conducting grid is being formed, its resistance will depend on the cobalt metal particle sizes, uniformity of random particle distribution on the interface surface, area and quality of contact between them. Large metallic particles provide a grid with lower resistivity. This explains lower resistance of Co$_n$(CoO)$_{100-n}$ produced in the inert atmosphere compared with the samples produced in the mixed atmosphere downstream of the percolation threshold.
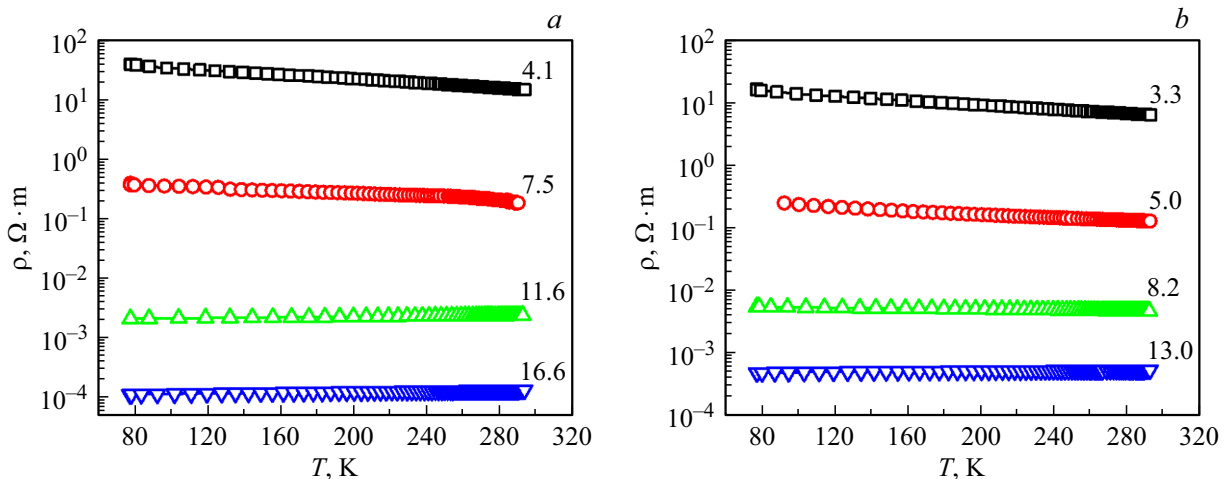
Figure 5. Models of structural Co$_n$(CoO)$_{100-n}$ composites synthesized in argon atmosphere (*a*) and mixed atmosphere Ar + O$_2$ (*b*).

Figure 7. temperature dependences of resistivity of thin $Co_n(CoO)_{100-n}$ films in initial state produced by sputtering in argon atmosphere (a) and mixed $Ar + O_2$ atmosphere (b).

Figure 6 shows thermo-emf-concentration dependences for $Co_n(CoO)_{100-n}$. All measured thermo-emf values are negative and their absolute value is lower than the thermo-emf of bulk cobalt at the specified temperatures (about $\sim 27 \mu V/K$ [17]). Analysis of the obtained dependences shows that, for composites sputtered in argon atmosphere, thermo-emf has its minimum (in absolute value) near the percolation threshold, and the dependence shapes generally remain the same when oxygen is injected in the sputtering atmosphere. The presence of oxygen in the sputtering atmosphere results in total reduction of thermo-emf in absolute value and shift of the minimum value towards lower metallic phase concentrations.

For composites upstream of the percolation threshold, the thermo-emf is governed, on the one hand, by direct electron tunneling from one metallic granule to another and, on the other hand, by hopping electrotransport on localized states of the CoO matrix [18]. In the first case, reduction of the tunnel gaps between the Co metal particles shall result in growth of the tunnel thermo-emf. Then with growth of the metallic phase, thermo-emf shall increase for $Co_n(CoO)_{100-n}$ samples upstream of the percolation threshold. Moreover, thermo-emf for the samples produced in the mixed argon-oxygen atmosphere shall be higher that for the samples produced in the argon atmosphere. Figure 6 shows that such dependences are not observed in our experiment suggesting that the thermo-emf of $Co_n(CoO)_{100-n}$ upstream of the percolation threshold is of the hopping type.

In the composites downstream of the percolation threshold, where thermo-emf is of diffusion type, oxidation of the cobalt metal granules causes reduction of their contact surface that may hinder the electron transport and, thus, result in decreased thermo-emf. Therefore, oxygen injection into the sputtering atmosphere can increase considerably the tunnel thermo-emf in the composites upstream of the

percolation threshold and the diffusion thermo-emf in the composites downstream of the percolation threshold.

Thus, the simultaneous analysis of the resistivity and thermo-emf dependences of thin films produced by sputtering in argon atmosphere and mixed $Ar + O_2$ atmosphere shows that oxygen injection into the chamber during sputtering causes mainly the change in electric properties due to the topological structural changes in $Co_n(CoO)_{100-n}$.

3.2. Temperature dependences of resistance of $Co_n(CoO)_{100-n}$

To identify the features of electrotransport of thin $Co_n(CoO)_{100-n}$ films, dependences of resistivity on temperature were examined and are shown in Figure 7 for thin $Co_n(CoO)_{100-n}$ films produced in argon and argon + oxygen atmosphere.

The investigations have shown that resistance is growing with temperature for thin $Co_n(CoO)_{100-n}$ films located at and downstream of the percolation threshold that is indicative of metallic conductivity mechanism on the grid formed by the metallic Co inclusions. To examine the heat treatment effect on the electric properties of the produced films, temperature dependences of resistivity were also investigated for thin $Co_n(CoO)_{100-n}$ films after heat treatment in vacuum at 520 K during 30 min (Figure 8).

For compositions located upstream of the percolation threshold, the resistance decreases with temperature growth. Moreover, it has been found that the resistance follows the „ 1/4 law“ ($\ln \rho \propto T^{-1/4}$) within $80-140$ K (figs. 9, 10) and the Arrhenius dependence ($\ln \rho \propto 1/T$) within $140-300$ K (Figures 11, 12).

If fulfilment of the „ 1/4 law“ is treated as a sign of hopping conductivity on the localized states in a narrow energy band near the Fermi level (Mott conductivity), then
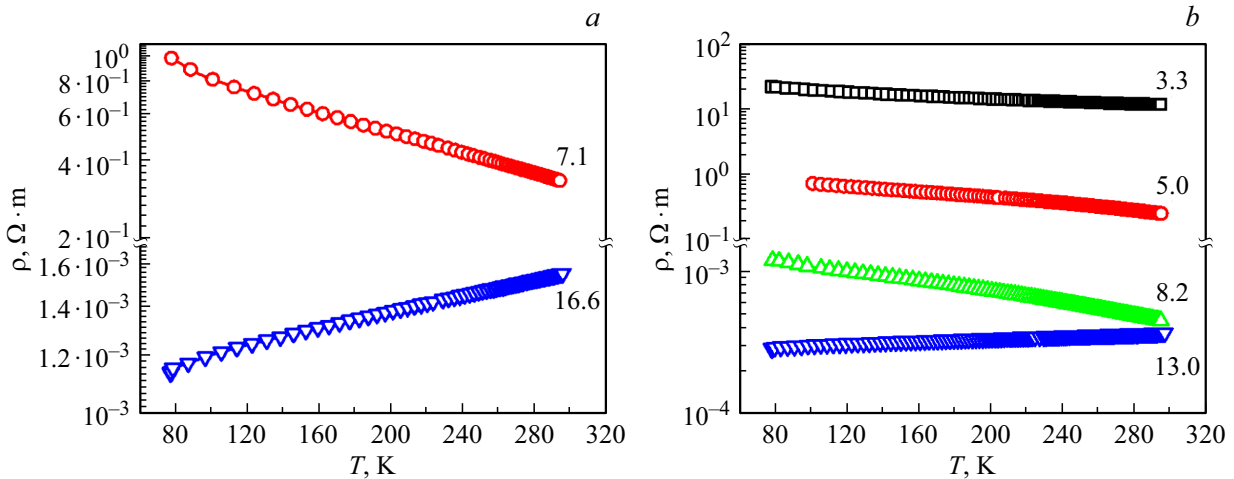
Figure 8. Temperature dependences of resistivity of thin Co$_n$(CoO)$_{100-n}$ films produced by sputtering in argon atmosphere (a) and mixed Ar + O$_2$ atmosphere (b) after heat treatment in vacuum at 520 K during 30 min.
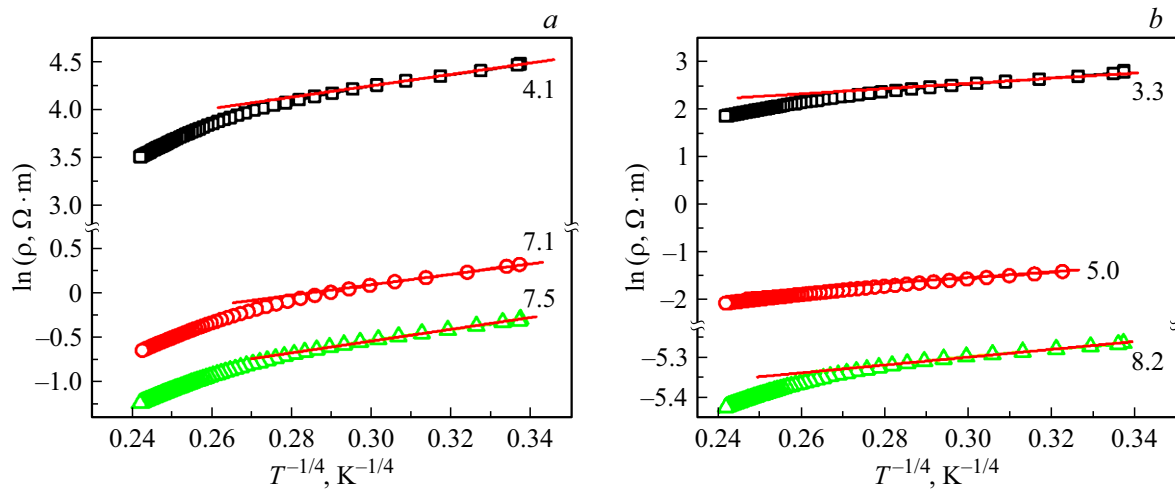

Figure 9. Temperature dependences of resistivity presented in coordinates $\ln\rho \propto T^{-1/4}$ for thin Co$_n$(CoO)Co$_n$ films in initial state produced by sputtering in argon atmosphere (a) and mixed Ar$_{100-n}$O$_2$ atmosphere (b).

the expression for conductivity is as follows [19]:

$$\sigma = e^2 \cdot R^2 \cdot v_{ph} \cdot g \cdot \exp\left(-\frac{B}{T}\right)^{1/4}, \qquad (1)$$

where

$$B = \frac{16}{a^3 \cdot k_B \cdot g(E_F)}, \qquad (2)$$

e — electron charge, R — hop distance, v_{ph} — interaction phonon spectrum factor, T — absolute temperature, $g(E_F)$ — density of states at the Fermi level, a — electron wave function localization radius, k_B — Boltzmann constant.

Figures 9 and 10 were used to determine B values for the examined film compositions. Knowing B and assuming that the charge carrier transport process is limited by hops between Co nanograins, localization radius $a \sim 5$ nm (average size of Co grains) is assumed to assess the density

of localized states. The obtained densities of states at the Fermi level for different thin film compositions are shown in Table 1.

We shall also estimate the average hop energy that shall be as follows for the hops with a variable hop distance:

$$W_M = \frac{1}{4}K_B T\left(\frac{T_{O_M}}{T}\right)^{1/4}. \qquad (3)$$

Using the following equation

$$R_M = \frac{3}{8}a\left(\frac{T_{O_M}}{T}\right)^{1/4} \qquad (4)$$

the average charge carrier hop distance was estimated at ~ 120 K (Table 1).

The estimates of hopping conductivity with a variable hop distance listed in Table 1 suggest that increasing concentration of the metallic Co phase results in the
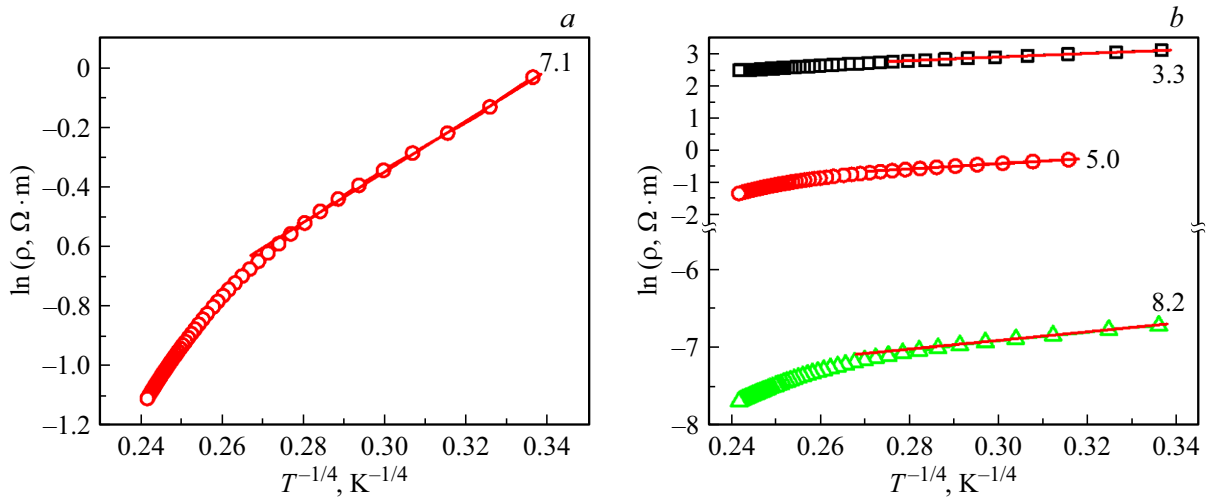
Figure 10. Temperature dependences of resistivity presented in coordinates $\ln\rho \propto T^{-1/4}$ for thin $Co_n(CoO)_{100-n}$ films produced by sputtering in argon atmosphere (a) and mixed $Ar + O_2$ atmosphere (b) after heat treatment in vacuum at 520 K during 30 min.
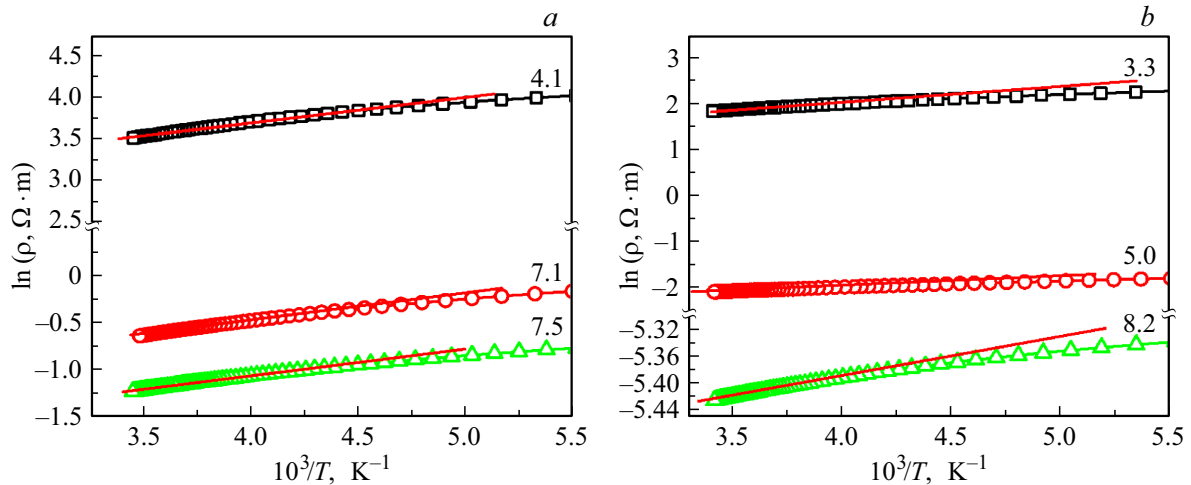

Figure 11. Temperature dependences of resistivity presented in coordinates $\ln\rho \propto 1/T$ of thin $_n(CoO)_{100-n}$ films in initial state produced by sputtering in argon atmosphere (a) and mixed $Ar + O_2$ atmosphere (b).

increased density of localized states near the Fermi level and reduced average hop distance. Heat treatment in vacuum at 520 K during 30 min results in decreasing density of localized states near the Fermi level and increasing average hop distance due to lower presence of defects in the CoO matrix of the examined composites between the Co metal inclusions. The states mentioned above are probably formed by the CoO matrix at the Co metal and CoO grain interface.

As mentioned above, the temperature dependences of resistivity for the examined thin films within $140-300$ K follow the Arrhenius dependence $(\ln\rho \propto 1/T)$ (Figures 11, 12).

If the designated temperature interval is treated as a region of hopping conductivity on the nearest neighbors, then, according to [19], the following equation shall be true

for the conductivity

$$\sigma = \sigma_0 \cdot \exp\left(\frac{W_{NNH}}{k_B T}\right), \qquad (5)$$

where W_{NNH} is the hop activation energy set for the hops on the nearest neighbors by the following equation

$$W_{NNH} = \frac{3}{4\pi R_0^3 g(E_F)}, \qquad (6)$$

where R_0 is the average distance between the nearest neighbors, $g(E_F)$ is the density of states at the Fermi level.

Using equations (5) and (6), estimate the hop activation energies from Figures 11 and 12. These results are given in Table 2.

Comparison of data in Tables 1 and 2 shows that the hop activation energy decreases in switching from the hopping
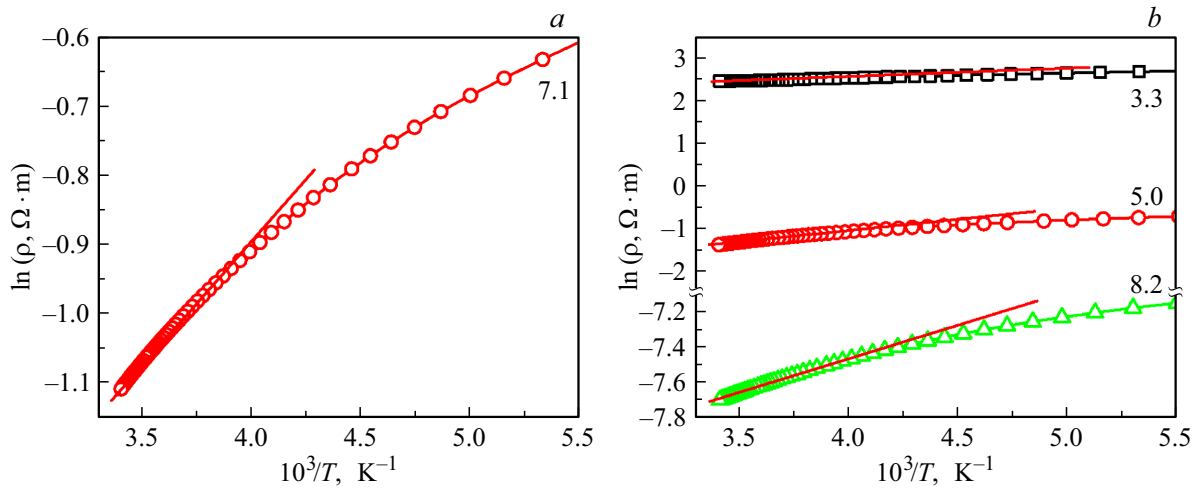
Figure 12. Temperature dependences of resistivity presented in coordinates $\ln\rho \propto 1/T$ for thin Co$_n$(CoO)$_{100-n}$ films produced by sputtering in argon atmosphere (*a*) and mixed Ar + O$_2$ atmosphere (*b*) after heat treatment in vacuum at 520 K during 30 min.

Table 1. Parameters of thin Co$_n$(CoO)$_{100-n}$ films calculated according to the hopping conductivity model of electrons with a variable hop length over the localized states within a narrow energy band near the Fermi level

Atmosphere at sputtering	n, at.%	$B^{1/4}$, K$^{1/4}$	B, K	$g(E_F)$, eV^{-1}·cm^{-3}	R_M at 120 K, nm	W_M, meV ($T = 120$ K)	$B^{1/4}$, K$^{1/4}$	B, K	$g(E_F)'$, eV^{-1}·cm^{-3}	R_M during 120 K, nm	W_M, meV ($T = 120$ K)
				Initial state					Heat treatment in vacuum $P_{res} = 2.5 \cdot 10^{-4}$ Torr $T = 520$ K		
Ar	4.1	6.78	2113	$9.2 \cdot 10^{20}$	3.8	5.3	−	−	−	−	−
	7.1	4.35	357	$5.5 \cdot 10^{21}$	2.5	3.4	8.47	5147	$3.8 \cdot 10^{20}$	4.8	6.6
	7.5	3.79	206	$9.5 \cdot 10^{21}$	2.1	3.0	−	−	−	−	−
Ar + O$_2$	3.3	4.96	606	$3.2 \cdot 10^{21}$	2.8	3.9	8.15	4412	$4.4 \cdot 10^{20}$	4.6	6.4
	5	4.16	299	$6.5 \cdot 10^{21}$	2.4	3.3	5.86	1179	$1.7 \cdot 10^{21}$	3.3	4.6
	8.2	3.35	127	$1.5 \cdot 10^{22}$	1.9	2.6	5.65	1019	$1.9 \cdot 10^{21}$	3.2	4.4

Table 2. Specifications of thin Co$_n$(CoO)$_{100-n}$ films calculated according to the nearest neighbor hopping conductivity model

Sputtering atmosphere	n, at.%	W_{NNH}, eV ($T = 140$ K)	R_0, nm	W_{NNH}, eV ($T = 140$ K)	R_0, nm
		Initial state		Heat treatment in vacuum $P_{res} = 2.5 \cdot 10^{-4}$ Torr at $T = 520$ K	
Ar	4.1	0.058	2.7	−	−
	7.1	0.055	0.3	0.026	0.026
	7.5	0.032	0.1	−	−
Ar + O$_2$	3.3	0.046	2.5	0.022	8.2
	5.0	0.029	2.2	0.012	5.6
	8.2	0.010	0.1	0.007	3.9

conductivity with variable hop distance to the nearest neighbor hops.

Since the conductivity with variable hop distance on localized states at the Fermi level that has been found before and the nearest neighbor conductivity shall take place within the same narrow energy band, and providing that the density of localized states is weakly dependent on temperature, then the data in Table 1 and equation (6) may be used to estimate the average distance between the nearest neighbors R_0 (Table 2).

Comparison of the data in Tables 1 and 2 suggests the following:

1. The average hop distance for the hopping conductivity with variable hop distance agrees with the distance between the nearest neighbors calculated for the nearest neighbor hopping conductivity.

2. Hop activation energies decrease in switching from the hopping conductivity with variable hop distance to the nearest neighbor hops.

In addition, assuming that for nearest neighbor hopping the width of localized state band near the Fermi level is approximately equal to the doubled hop activation energy, then Table 2 suggests that the width of this band decreases with increasing Co content.

Thus, the review of the temperature dependences of resistivity of thin $Co_n(CoO)_{100-n}$ films in initial state and after heat treatment has shown that there is no quality change in the electrotransport mechanisms. The heat treatment effect is limited to quantity changes in typical parameters of the corresponding mechanisms.

Conclusion

1. The method of ion-beam composite target sputtering in argon and mixed argon-oxygen atmosphere was used to synthesize heterogenous thin $Co_n(CoO)_{100-n}$ films. Analysis of the concentration dependences of resistivity and thermo-emf has shown that the obtained system is of percolation type. It has been shown that oxygen injection into the sputtering chamber moves the percolation threshold position towards lower metallic phase concentrations that is associated with the film morphology when small Co metal nanoparticles are located at the boundaries of large CoO particles as well as with reduced size of metallic phase inclusions.

2. Temperature dependences of resistivity of the synthesized thin $Co_n(CoO)_{100-n}$ films have been examined experimentally. It has been shown that, when the metallic phase is upstream of the percolation threshold in the temperature range of $80-140$ K, the hopping conductivity on the localized states near the Fermi level with variable hop distance, that is replaced by the nearest neighbor hops in the temperature range of $140-300$ K, is the dominating charge transport mechanism. For thin $Co_n(CoO)_{100-n}$ films located downstream of the percolation threshold, the conductivity depends on the metallic granule grid and has a positive temperature coefficient of resistivity.

Conflict of interest

The authors declare that they have no conflict of interest.

References

[1] T. Wen, K.M. Krishnan. J. Phys. D: Appl. Phys., **44** (39), 393001 (2011). DOI: 10.1088/0022-3727/44/39/393001

[2] V. Baltz, A. Manchon, M. Tsoi, T. Moriyama, T. Ono, Y. Tserkovnyak. Rev. Mod. Phys., **90** (1), 015005 (2018). DOI: 10.1103/RevModPhys.90.015005

[3] Q. Wu, L. Yang, X. Wang, Z. Hu. Adv. Mater., **32** (27), 1904177 (2019). DOI: 10.1002/adma.201904177

[4] Yu. Sun, C.R. Sullivan, W. Li, D. Kopp, F. Johnson, S.T. Taylor. IEEE Trans. Magn., **43** (12), 4060 (2007). DOI: 10.1109/TMAG.2007.907503

[5] L.V. Spivak, A.V. Sosunov, N.E. Shchepina. Tech. Phys. Lett., **48** (8), 66 (2022). DOI: 10.21883/TPL.2022.08.55066.19258

[6] D. Yao, C.G. Levey, R. Tian, C.R. Sullivan. IEEE Trans. Power Electron., **28** (9), 4384 (2013). DOI: 10.1109/TPEL.2012.2233760

[7] Z. Ma, F. Jing, Y. Fan, J. Li, Y. Zhao, G. Shao. J. Alloys Compd., **789**, 71 (2019). DOI: 10.1016/J.JALLCOM.2019.03.035

[8] M. Baikousi, O. Kostoula, I. Panagiotopoulos, T. Bakas, A.P. Douvalis, I. Koutselas, A.B. Bourlinos, M.A. Karakassides. Thin Solid Films, **520** (1), 159 (2011). DOI: 10.1016/j.tsf.2011.06.110

[9] H.I. Blythe, V.M. Fedosyuk, O.I. Kasyutich. Mater. Lett., **26** (1−2), 69 (1996). DOI: 10.1016/0167-577X(95)00207-3

[10] D.A. Petrov, I.S. Edelman, R.D. Ivantsov. Solid State Phenom., **215**, 214 (2014). DOI: 10.4028/www.scientific.net/SSP.215.214

[11] V.G. Myagkov, L.E. Bykova, O.A. Bayukov, V.S. Zhigalov, I.A. Tambasov, S.M. Zharkov, A.A. Matsynin, G.N. Bondarenko. J. Alloys Compd., **636**, 223 (2015). DOI: 10.1016/j.jallcom.2015.02.012

[12] S.A. Gridnev, Yu.E. Kalinin, A.V. Sitnikov, O.V. Stogney. *Nelineynye yavleniya v nano- i mikrogeterogennykh sistemakh* (Binom, Laboratoriya znaniy, M., 2012) (in Russian).

[13] N.T. Gladkikh, S.V. Dukarov, A.P. Kryshtal, V.I. Larin, V.N. Sukhov, S.I. Bogatyrenko. *Poverkhnostnye yavleniya i fazovye prevrashcheniya v kondensirovannykh plenkakh*, pod red. N.T. Gladkikh (Kharkov: KhNU im. V.N. Karazina, 2004), s. 276.

[14] P. Scherer. Nachrichten von der Gesellschaft der Wissenschaften zu Göttingen, Mathematisch-Physikalische Klasse, **2**, 98 (1918)

[15] Yu.E. Kalinin, A.V. Sitnikov, O.V. Stogney. *Transportnye svoistva nanokompozitov metall-dielektrik* (Vestnik VGTU, 2007), t. 3 (11), s. 6−17.

[16] I.V. Zolotukhin, Yu.E. Kalinin, O.V. Stogney. *Novye napravleniya fizicheskogo materialovedeniya: Uchebnoe posobie* (Isd-vo Voronezhskogo gos. un-ta, Voronezh, 2000) (in Russian)

[17] A.P. Babichev, N.A. Babushkina, A.M. Bratkovsky, M.E. Brodov, M.V. Bystrov, B.V. Vinogradov, L.I. Vinokurova, E.B. Gelman, A.P. Geppe, I.S. Grigoriev, K.G. Gurtovoy, V.S. egorov, A.V. Eletsky, L.K. Zarembo, V.Yu. Ivanov. *Fizicheskie velichiny: Spravochnik*, pod red. I.S. Grigor'eva, E.Z. Melikhova (Energoatomizdat, M., 1991) (in Russian).

[18] V.A. Belousov, Yu.E. Kalinin, A.V. Sitnikov. Phys. Solid State, **49** (10), 1848 (2007) DOI: 10.1134/S1063783407100071

[19] N.F. Mott, E.A. Davies. *Electron Processes in Non-Crystalline Materials* (Clarendon, Oxford, 1979)

Translated by Ego Translating